



# Investigating the role of stratospheric ozone as a driver of inter-model spread in CO<sub>2</sub> effective radiative forcing.

Rachael E. Byrom<sup>1</sup>, Gunnar Myhre<sup>1</sup>, Dirk Olivié<sup>2</sup>, Michael Schulz<sup>2</sup>

<sup>1</sup>CICERO, Oslo, 0318, Norway

5 <sup>2</sup>Norwegian Meteorological Institute, Oslo, 0313, Norway

*Correspondence to:* Rachael E. Byrom (rachael.byrom@cicero.oslo.no)

**Abstract.** Addressing the cause of inter-model spread in carbon dioxide (CO<sub>2</sub>) radiative forcing is essential for reducing uncertainty in estimates of climate sensitivity. Recent studies demonstrate that a large proportion of this spread arises from variance in model base state climatology, particularly the specification of stratospheric temperature, which itself plays a dominant role in determining the magnitude of CO<sub>2</sub> forcing.

Here we investigate stratospheric ozone (O<sub>3</sub>) as a cause of inter-model differences in stratospheric temperature, and hence its role as a contributing factor to spread in CO<sub>2</sub> radiative forcing. We use the Norwegian Earth System Model 2 (NorESM2) to analyse the impact of systematic increases/decreases in stratospheric O<sub>3</sub> on the magnitude of 4xCO<sub>2</sub> effective radiative forcing (ERF) and its components.

15 Firstly, we demonstrate that accurate estimation of instantaneous radiative forcing requires the use of host-model radiative transfer calculations. Secondly, we show that a 50% increase and decrease in stratospheric O<sub>3</sub> concentration leads to significant differences in base state stratospheric temperature, ranging from +6 K to -9 K, respectively. However, this does not result in a correspondingly large spread in CO<sub>2</sub> ERF due to the impact of base-state stratospheric temperature on the emission of outgoing longwave radiation and the spectral overlap of CO<sub>2</sub> and O<sub>3</sub>. We conclude that inter-model differences in stratospheric  
20 O<sub>3</sub> concentration are therefore not predominantly responsible for inter-model spread in CO<sub>2</sub> ERF.

## 1 Introduction

Effective radiative forcing (ERF) quantifies the top-of-atmosphere (TOA) perturbation to the Earth's energy balance imposed by a forcing mechanism, such as CO<sub>2</sub>, aerosols or solar irradiance. It includes the instantaneous radiative forcing (IRF; i.e., the initial radiative response to the perturbation) and the subsequent radiative effect of adjustments in tropospheric and  
25 stratospheric temperature, water vapour, surface albedo and clouds, which each cause an impact on TOA radiative fluxes (Myhre et al., 2013; Boucher et al., 2013; Sherwood et al., 2015; Forster et al., 2021).

ERF can be expressed simply (following e.g., Chung and Soden 2015a; Smith et al., 2018) as:



$$ERF = IRF + A_{T_{Strat}} + A_{T_{Trop}} + A_{H_2O} + A_{\alpha} + A_c + \epsilon, \quad (1)$$

30

whereby ERF is the net (shortwave plus longwave) change in downward TOA flux ( $W m^{-2}$ ), IRF is the direct net change in downward TOA flux ( $W m^{-2}$ ),  $A_x$  is the radiative adjustment from stratospheric temperature ( $T_{Strat}$ ), tropospheric temperature ( $T_{Trop}$ ), water vapour ( $H_2O$ ), surface albedo ( $\alpha$ ) and clouds (c), with  $\epsilon$  representing a non-linear residual term.

35 ERF is used extensively to compare the relative strength of different forcing agents. Historically, quantifying the climate impact of a given agent commonly relied solely on diagnosing its IRF or stratospheric temperature adjusted radiative forcing (SARF, e.g., Ramaswamy et al., 2019). However, given that additional so-called ‘adjustments’ develop from the initial radiative perturbation and impact the TOA imbalance, it is also necessary to include them in the radiative forcing framework. Consequently, this has been shown to improve the utility of the radiative forcing metric in predicting global-mean surface  
40 temperature change ( $\Delta T_s$ ), ultimately due to a more realistic separation of forcing from surface-temperature driven feedbacks (e.g. Sherwood et al., 2015; Marvel et al., 2016; Richardson et al., 2019). Adjustments therefore form an important component of climate change assessment and necessitate the use of climate model integrations to simulate the radiative response of tropospheric and land-surface changes to TOA energy imbalance, in addition to the traditional diagnostic of IRF or SARF, which can be calculated using offline radiative transfer codes or simplified expressions (e.g. Hansen et al., 1988; Myhre et al.,  
45 1998; Etminan et al., 2016; Meinshausen et al., 2020). This makes ERF considerably more computationally-expensive to estimate and introduces more model diversity driven uncertainty. The use of different methods to calculate ERF further complicates inter-model comparison, with some studies opting to diagnose the forcing from fixed sea-surface temperature (SST) and sea ice simulations (Hansen et al., 2005), or alternatively, by regressing TOA irradiance against global surface temperature change (Gregory et al., 2004; see Forster et al., 2016).

50

For  $CO_2$ , inter-model spread in ERF remains an ongoing issue. Smith et al. (2020a) report a  $4xCO_2$  ERF range of 7.3-8.9  $W m^{-2}$  for 17 CMIP6 (Coupled Model Intercomparison Project Phase 6; Eyring et al., 2016) models contributing to the Radiative Forcing Model Intercomparison Project (RFMIP; Pincus et al., 2016), which aims to achieve accurate characterisation of ERF through consistent diagnosis with the fixed-SST method (Forster et al., 2016). Whilst this spread has been reduced compared  
55 to earlier analysis of 13 CMIP5 models (Kamae and Watanabe 2012; see Smith et al., 2020a Fig. 5), identifying and remedying the exact nature of  $CO_2$  ERF diversity is an active area of research (e.g., Soden et al., 2018; Pincus et al., 2016; Smith et al., 2020a). Several studies show that model differences in the magnitude of IRF contributes significantly (e.g., Zhang and Huang 2014; Chung and Soden 2015b; Andrews et al., 2015), arising either from radiative transfer parameterisation error (e.g., Collins et al., 2006; Pincus et al., 2015) and/or differences in model base state climatology (Pincus et al., 2020; Jeevanjee et al., 2021).  
60 Recently, He et al., (2023) more specifically attribute this base state dependence to stratospheric temperature. They report a significant correlation between  $4xCO_2$  IRF and 10 hPa air temperature in CMIP5/6 models, demonstrating that biases in



stratospheric temperature play a leading role in causing inter-model CO<sub>2</sub> IRF spread. Given that IRF accounts for around 60% of CO<sub>2</sub> ERF and that stratospheric cooling is its dominant adjustment (Myhre et al., 2013; Smith et al., 2018), examining potential causes of model differences in stratospheric temperature presents a clear opportunity to further current understanding.

65

Here, we perform idealised experiments (Section 2) to investigate the role of stratospheric O<sub>3</sub> as a driver of inter-model diversity in stratospheric temperature, and hence its role as a driver of spread in CO<sub>2</sub> ERF. First, we examine 4xCO<sub>2</sub> ERF and compare our results to previous estimates, with a particular focus on the diagnosis of IRF and  $T_{Strat}$  (Section 3). We then investigate the impact of stratospheric O<sub>3</sub> specification on each component of 4xCO<sub>2</sub> ERF (Section 4).

70

## 2 Models, experiments and methods

We use atmosphere-only simulations from NorESM2-MM (Seland et al., 2020) to calculate ERF following an abrupt quadrupling of CO<sub>2</sub> relative to pre-industrial (1850) conditions (see Text S1 in the Supplement for further detail on model configuration). This model is used to perform a baseline (control) integration and a perturbed (4xCO<sub>2</sub>) integration using prescribed SST and sea-ice extent climatologies; hence we use the fixed-SST method to diagnose forcing as recommended by RFMIP (Pincus et al., 2016) whereby ERF is calculated as the difference in TOA net radiative flux between the perturbed and control simulations. Integrations are run for 30 years, with years 6 to 30 used for analysis in Section 3. This simulation length was chosen to allow for better comparison of our results against the 30-year NorESM2-MM 4xCO<sub>2</sub> ERF experiments of Smith et al. (2020a).

80

We perform two further 4xCO<sub>2</sub> ERF experiments whereby stratospheric O<sub>3</sub> is increased by 50% (Strat O<sub>3</sub>x1.5) and decreased by 50% (Strat O<sub>3</sub>x0.5) relative to its pre-industrial concentration. As in the ‘standard’ 4xCO<sub>2</sub> ERF experiment described above, stratospheric O<sub>3</sub> fields are prescribed using output from the Community Earth System Model version 2 - Whole Atmosphere Community Climate Model version 6 (CESM2-WACCM6; Gettelman et al., 2019) as zonally-averaged 5 day fields (Fig. S1). A linearly varying tropopause (from 100hPa at the equator to 300 hPa at the poles) is used to delineate the stratosphere and troposphere (Soden et al., 2008, Smith et al. 2018). O<sub>3</sub> concentrations above this boundary are multiplied by 1.5 and 0.5 to increase and decrease levels by 50%, respectively. These simulations are run for 15 years to reduce computational expense, with years 6 to 15 of each integration used for analysis (Section 4). Table S1 summarises all experiments.

90

IRF is calculated using the Parallel Offline Radiative Transfer (PORT; Conley et al., 2013) code. This code isolates the radiative transfer scheme employed by NorESM2-MM (i.e., RRTMG, Iacono et al., 2008) to provide stand-alone radiation diagnostics. It is used here to perform two sets of radiative transfer calculations for each experiment listed in Table S1; a baseline (control) simulation and a perturbed (4xCO<sub>2</sub>) simulation, which are both run using climatology from the corresponding



ERF control integration. Simulations are run for 16 months with the last 12 months used to diagnose annual-mean IRF as the  
95 difference in TOA net radiative flux between the perturbed and control run.

Corresponding radiative adjustments are quantified using radiative kernels (Soden et al., 2008). Summarising the more detailed  
description given by Smith et al. (2018), these characterise the change in TOA radiative flux  $\Delta R$  (either shortwave or  
longwave) following a unit change in a state variable ( $\Delta x$ ), e.g., stratospheric temperature, surface albedo or clouds. They are  
100 constructed by running a climate model's offline radiative transfer code twice, once with a baseline climatology and again  
with a unit change in  $x$  to calculate  $\Delta R$ . The radiative kernel ( $K_x$ ) is given by:

$$K_x = \frac{\partial R}{\partial x}. \quad (2)$$

The corresponding adjustment ( $A_x$ ) is then quantified as:

105

$$A_x = K_x(x_p - x_c), \quad (3)$$

whereby  $x_p - x_c$  represents the difference in  $x$  between the perturbed and control atmosphere-only climate model  
integrations, respectively. Here,  $A_x$  is calculated using output from NorESM2-MM with radiative kernels derived from three  
models: the Community Earth System Model 1-Community Atmosphere Model 5 (CESM-CAM5, Pendergrass et al., 2018),  
110 the Hadley Centre Global Environment Model 3-GA7.1 (HadGEM3-GA7.1, Smith et al., 2020b), and the European Centre for  
Medium-Range Weather Forecasts (ECMWF)-Oslo model (Myhre et al., 2018). We use kernels to calculate all adjustments  
given in Eq. (1) except for  $A_c$ . Since we calculate IRF directly using PORT, this allows us to diagnose  $A_c$  as a residual by  
subtracting the IRF and the sum of all other adjustments from the ERF (with the assumption that  $\epsilon$  is zero). This differs from  
alternate methods used to calculate  $A_c$  such as the kernel-difference method, which involves differencing all-sky and clear-sky  
115 fluxes (e.g., Soden et al., 2008; Smith et al., 2018; Smith et al., 2020a), and the approximate partial radiative perturbation  
(APRP) method, which estimates shortwave cloud responses from climate model diagnostics (Zelinka et al., 2014; Smith et  
al., 2018). Additionally, we also calculate the adjustment due to surface temperature change ( $A_{T_S}$ ) since land-surface  
temperatures are allowed to respond to the forcing in our simulations given the difficulty in prescribing fixed surface  
temperatures. Several studies follow this approach (e.g., Hansen et al., 2005; Forster et al., 2016; Smith et al., 2018). Generally,  
120 methods that correct for this response produce a slightly larger ERF following a CO<sub>2</sub> perturbation (Smith et al., 2020a; Andrews  
et al., 2021). We use the same tropopause definition as above to delineate  $A_{T_{Strat}}$  and  $A_{T_{Trop}}$ .



### 3 The importance of a direct calculation of IRF and the dependence of $A_{T_{Strat}}$ on radiative kernel choice

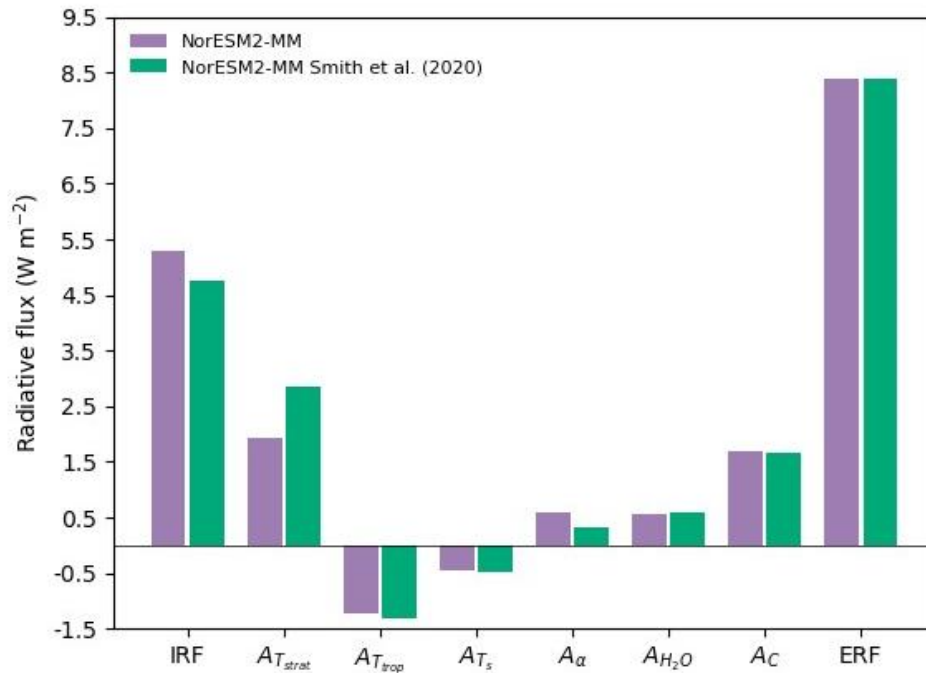
Figure 1a (purple bars) shows the resulting NorESM2-MM ERF, IRF and adjustments. For comparison, corresponding data from the NorESM2-MM 4xCO<sub>2</sub> ERF experiment of Smith et al. (2020a) is also shown (green bars). As expected, the magnitude of ERF is near-equal in each experiment, at 8.40 W m<sup>-2</sup> (purple bar) and 8.38 W m<sup>-2</sup> (green bar). The difference of 0.02 W m<sup>-2</sup> is likely attributable to differences in the time-period used to average model output, or to the use of alternate initial conditions and computing machine architecture, given that all other aspects of simulation design were implemented identically (see Section 2 and Smith et al., 2020a, Section 2).

130

135



a)



b)

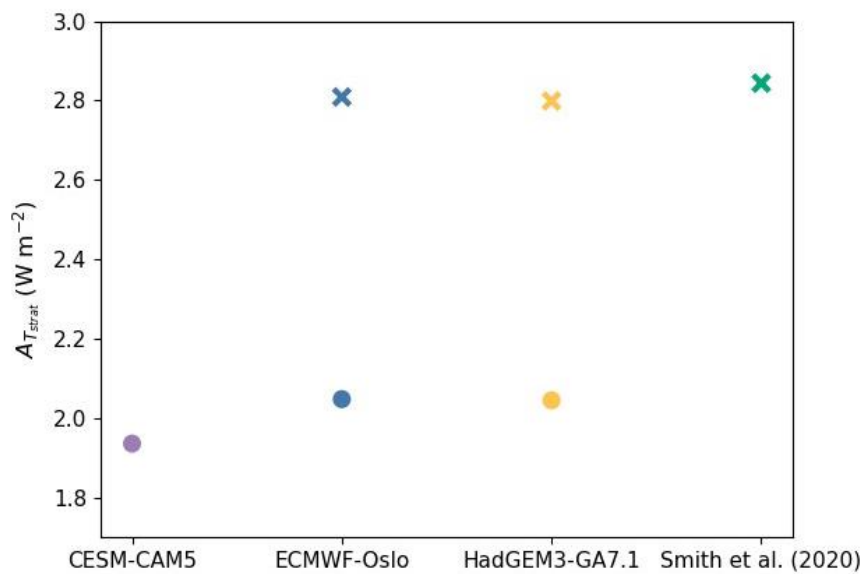


Figure 1: a) NorESM2-MM 4xCO<sub>2</sub> ERF and its components (purple bars) with IRF calculated using PORT and adjustments diagnosed using the CESM-CAM5 kernels. Green bars show corresponding data from Smith et al. (2020a), whereby the ERF for the same perturbation has been calculated from 30-year simulations of NorESM2-MM with adjustments



calculated using the HadGEM3-GA7.1 radiative kernels and with IRF estimated as the residual of ERF minus total adjustments. b) Comparison of NorESM2-MM  $A_{T_{Strat}}$  when calculated using different radiative kernels. Filled circles represent  $A_{T_{Strat}}$  calculated following the methodology outlined in Section 2, whereby NorESM2-MM output is interpolated onto the given radiative kernel pressure levels but not extrapolated to kernel pressure levels outside of the NorESM2 uppermost and lowermost pressures. Crosses represent the magnitude of  $A_{T_{Strat}}$  if such extrapolation is performed for the ECMWF-Oslo and HadGEM3-GA7.1 kernels and the value given by Smith et al. (2020a) (which used the HadGEM3-GA7.1 kernel).

140

Figure 1a further shows that the magnitude of IRF varies notably between both experiments demonstrating a dependence on the diagnostic method of choice. When calculated directly using PORT, the IRF is  $0.54 \text{ W m}^{-2}$  larger than when estimated as the difference between ERF and the sum of adjustments (as in Smith et al. 2020a), comparing  $5.30 \text{ W m}^{-2}$  (purple bar) and  $4.76 \text{ W m}^{-2}$  (green bar). This demonstrates the necessity of using an offline version of a model's own radiative transfer code to calculate IRF and highlights the possibility for error in studies that derive this forcing as a residual. We further note the close agreement in  $A_c$ , which interestingly occurs despite the use of different methods to calculate it. In Smith et al. (2020a)  $A_c$  is estimated using the APRP approach with liquid water path adjustment and with offline monthly-mean partial radiative perturbation calculations. Whereas in our approach,  $A_c$  is calculated as a residual using accurate host-model radiative transfer calculations (IRF) and host-model radiative kernels for accurate calculations of non- $A_c$  terms.

150

The stratospheric temperature adjustment is strong and positive as anticipated due to the process of stratospheric cooling following an increase in  $\text{CO}_2$  concentration (e.g. Myhre et al., 2013; Smith et al., 2018; Forster et al., 2021). However, there is a clear difference when comparing the value reported here ( $1.94 \text{ W m}^{-2}$ , purple bar) against Smith et al. (2020a;  $2.84 \text{ W m}^{-2}$ , green bar). Because  $A_{T_{Trop}}$  is similar between both experiments ( $-1.23 \text{ W m}^{-2}$  vs  $-1.32 \text{ W m}^{-2}$ ) it can be deduced that the

155

difference in magnitude of  $A_{T_{Strat}}$  is not predominantly driven by the choice of tropopause definition (in Smith et al. (2020a) this is based on the World Meteorological Organization definition of a lapse-rate tropopause, whereby geopotential height is used as an approximation of geometric height on model pressure levels in the control integration). Instead, the difference in  $A_{T_{Strat}}$  stems from the use of different radiative kernels (i.e., CESM-CAM5 vs HadGEM3-GA7.1) and the method of applying model output in the  $A_{T_{Strat}}$  calculation. For our derivation of  $A_{T_{Strat}}$  we interpolate NorESM2-MM output to the 30 CESM-CAM5 kernel pressure levels, where 3.64 hPa is the highest level. Even though this is a 'low-top' kernel, this matches the highest level of NorESM2-MM output meaning that the use of this kernel in the  $A_{T_{Strat}}$  calculation captures all of the stratospheric cooling occurring in NorESM2-MM following a  $4\times\text{CO}_2$  perturbation. Alternatively, Smith et al. (2020a) use the HadGEM3-GA7.1 radiative kernel, which itself has been interpolated from a native vertical resolution of 85 pressure levels (up to around 0.005 hPa) to the standard 19 CMIP6 pressure levels, with an upper bound of 1 hPa. Smith et al. (2020a) derive

165

$A_{T_{Strat}}$  by using model output that has been interpolated and extrapolated to these 19 CMIP6 pressure levels. This therefore



extends stratospheric temperatures in NorESM2-MM above the model's highest level of 3.64 hPa to 1 hPa. Whilst this method better accounts for outgoing radiation emitted to space from the upper stratosphere for each unit change in temperature, it does not represent the actual adjustment modelled by NorESM2-MM.

170 Figure 1b (filled circles) further demonstrates this issue by comparing the magnitude of  $A_{T_{Strat}}$  calculated by applying our NorESM2-MM output to two additional kernels: ECMWF-Oslo and HadGEM3-GA7.1. The ECMWF-Oslo kernel has 60 pressure levels, with a high resolution in the stratosphere extending to 0.1 hPa, and as described above, the HadGEM3-GA7.1 utilises the standard CMIP6 19 pressure levels. When we interpolate (but do not extrapolate) NorESM2-MM output onto these pressure levels, the use of both ECMWF-Oslo and HadGEM3-GA7.1 results in an adjustment similar to that given by CESM-  
175 CAM5, at  $2.05 \text{ W m}^{-2}$  (blue and yellow filled circles). However, when NorESM2-MM output is both interpolated and extrapolated to the upper stratospheric levels of the ECMWF-Oslo and HadGEM3-GA7.1 kernels, the adjustment is notably stronger (and in closer agreement with Smith et al. 2020a) at around  $2.80 \text{ W m}^{-2}$  (blue and yellow crosses). The importance of the vertical resolution of stratosphere has been stated previously in studies quantifying the magnitude of  $A_{T_{Strat}}$  to a  $\text{CO}_2$  forcing. Notably, Smith et al. (2018) demonstrate that disagreement in  $2\times\text{CO}_2$   $A_{T_{Strat}}$  is dependent on whether a given kernel  
180 has high stratospheric resolution (e.g., ECMWF-Oslo) and if the model output is also highly resolved in the stratosphere. Smith et al. (2020b) further report that kernels based on a high-top atmospheric model with a large number of native pressure levels have a pronounced increase in the magnitude and rate of emitted radiation at 5 hPa and 1 hPa. Here, the difference between the 'extrapolated' (blue and yellow crosses) and 'not-extrapolated'  $A_{T_{Strat}}$  values (blue and yellow circles) in Fig. 1b infers that around  $0.75 \text{ W m}^{-2}$  of 'additional' stratospheric temperature adjustment occurs between the model top and the upper  
185 pressure limit of the ECMWF-Oslo and HadGEM3-GA7.1 kernels (0.1 hPa and 1 hPa, respectively). This therefore supports previous studies that highlight the significance of vertical stratospheric resolution on  $A_{T_{Strat}}$  and further demonstrates that the choice and method of applying a radiative kernel can substantially impact results. Opting to use a radiative kernel that has been constructed from the same atmospheric model as the  $\text{CO}_2$  forcing simulations in question will more accurately represent the magnitude of  $A_{T_{Strat}}$  simulated within that given model. This also ensures that the calculation of  $A_{T_{Strat}}$  is based entirely on  
190 one underlying radiative transfer code, which eliminates any uncertainty in the magnitude of  $A_{T_{Strat}}$  that could occur if the kernel and model output were derived from two different parameterisations.

## 4 Stratospheric $\text{O}_3$ experiments

### 4.1 Impact of $\text{O}_3$ perturbations on stratospheric temperature

$\text{O}_3$  plays an important role in driving the thermal structure of the stratosphere due to strong absorption of ultraviolet radiation and absorption and emission of thermal-infrared (TIR) radiation. Figure 2 (left) shows the effect of a 50% increase in  
195 stratospheric  $\text{O}_3$  concentration on zonal-mean atmospheric temperature in the control integration of NorESM2-MM. A strong





increase in stratospheric temperature is evident, consistent with enhanced absorption of solar radiation and hence enhanced solar heating rates. The peak increase in temperature occurs in the lower stratosphere centered across the equatorial region, co-located with high insolation. Here the maximum  $\Delta T$  reaches 5.8 K. Similarly, decreasing stratospheric  $O_3$  concentration by 50% results in reduced absorption of solar radiation, reduced solar heating rates and a strong cooling of the stratosphere (Fig. 2, right). As above, the peak temperature decrease occurs in the lower stratosphere across the equator, with a maximum  $\Delta T$  of -9 K. The impact of reduced stratospheric  $O_3$  also propagates into the troposphere (primarily between  $70^\circ$ - $90^\circ$ N/S), due to more downward solar irradiance reaching the lower levels of the atmosphere where enhanced absorption and heating can take place. Considering the high correlation between  $4xCO_2$  IRF and 10 hPa air temperature reported by He et al. (2023), we note that at this level in particular  $\Delta T$  largely increases by  $\geq 3$  K in the ‘Strat  $O_3 \times 1.5$ ’ case (Fig 2., left) and largely decreases by  $\geq 4$  K in the ‘Strat  $O_3 \times 0.5$ ’ case (Fig 2., right).

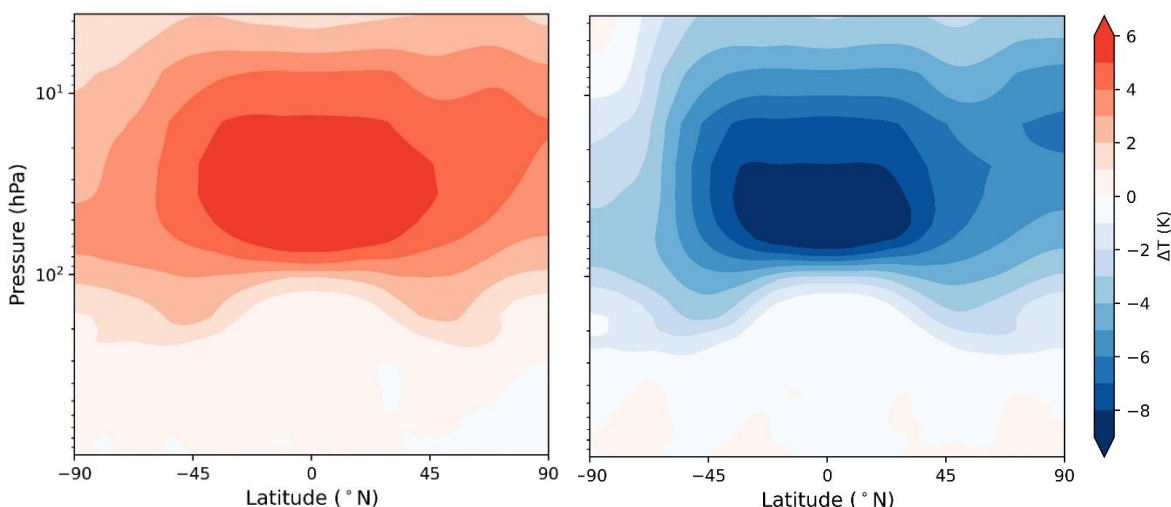


Figure 2: Zonal-mean difference in atmospheric temperature between the control integration of ‘Strat  $O_3 \times 1.5$ ’ and the control integration of the ‘standard’  $4xCO_2$  ERF simulation (left) and between the control integration of ‘Strat  $O_3 \times 0.5$ ’ and the control integration of the ‘standard’  $4xCO_2$  ERF simulation (right).

#### 4.2 Impact of stratospheric $O_3$ perturbations on $4xCO_2$ ERF and components

Figure 3 compares ERF, IRF and the individual adjustments for the ‘standard’  $4xCO_2$ , ‘Strat  $O_3 \times 1.5$ ’ and ‘Strat  $O_3 \times 0.5$ ’ experiments. As shown, increasing stratospheric  $O_3$  by 50% has negligible impact on the magnitude of  $4xCO_2$  ERF in NorESM2-MM, resulting in an identical forcing of  $8.48 \text{ W m}^{-2}$  compared to the ‘standard’ case (dark-orange bar). Similarly, the effect of decreasing stratospheric  $O_3$  by 50% has a marginal effect on  $4xCO_2$  ERF, increasing the forcing by just  $0.2 \text{ W m}^{-2}$



215 <sup>2</sup> relative to the ‘standard’ case. Evidently, the impact of increased/decreased O<sub>3</sub> concentration on stratospheric temperature (Fig. 2) does not result in a marked effect on ERF. In all three cases NorESM2-MM simulates a considerably larger ERF than the 17 CMIP6 multi-model mean of 7.98 W m<sup>-2</sup> reported by Smith et al. (2020a).

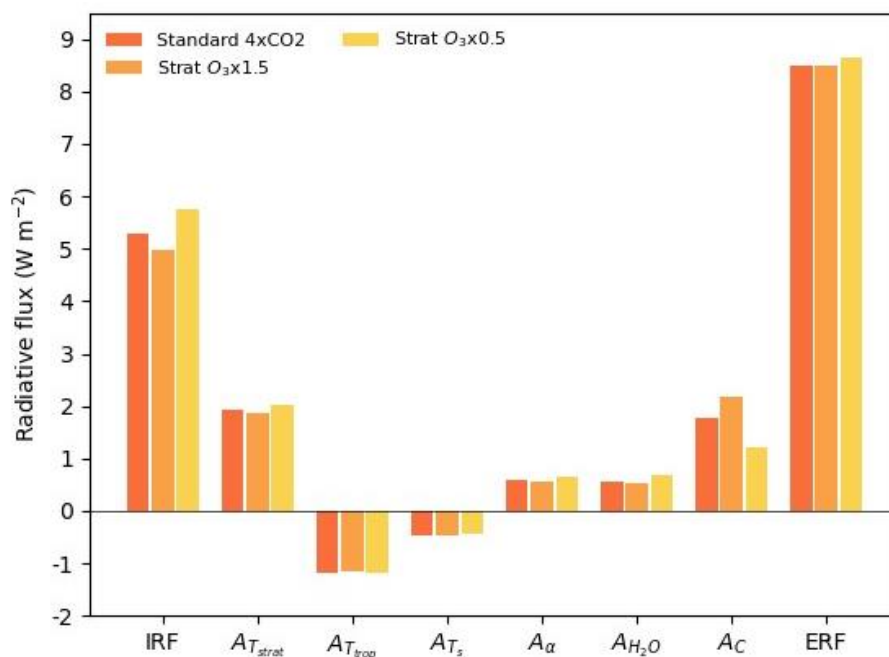


Figure 3: Comparison of NorESM2-MM ‘standard’ 4xCO<sub>2</sub> ERF, IRF and adjustments against ERF, IRF and adjustments diagnosed from the ‘Strat O<sub>3</sub>x1.5’ and ‘Strat O<sub>3</sub>x0.5’ experiments. All adjustments are derived using the CESM-CAM5 kernels and all components are derived from the average of years 6-15 of NorESM2-MM output, hence the values for the ‘standard’ 4xCO<sub>2</sub> case shown here differ slightly to those shown in Fig. 1.

220 Analysis of  $A_{T_{Strat}}$  further demonstrates that these experiments do not cause a significant effect on the magnitude of temperature adjustment throughout the stratosphere, producing just a 3% decrease and 4% increase in this component for the ‘Strat O<sub>3</sub>x1.5’ and ‘Strat O<sub>3</sub>x0.5’ cases, respectively. Apart from  $A_C$  (which is derived here as a residual term), the largest impact occurs on the IRF which increases by 9% and decreases by 6% when stratospheric O<sub>3</sub> is reduced and enhanced relative to the ‘standard’ experiment. The IRF across all three experiments ranges from 4.9 – 5.7 W m<sup>-2</sup> resulting in a spread of 0.8 W m<sup>-2</sup>. This is much smaller than the spread of 4 W m<sup>-2</sup> (ranging from 4 – 8 W m<sup>-2</sup>) reported by He et al. (2023) for online double-  
225 call experiments of 4xCO<sub>2</sub> IRF calculated with base-states from the Atmospheric Model Intercomparison Project (AMIP) for 12 CMIP5/6 models.



The effect on IRF can be explained principally by the impact of  $O_3$  increases/decreases on base-state stratospheric temperature and also by the spectral overlap of  $CO_2$  and  $O_3$ . In the ‘Strat  $O_3 \times 0.5$ ’ case for example, the reduced  $O_3$  concentration induces  
230 cooling of the stratosphere, which reduces the emission of outgoing TIR irradiance at the TOA and makes the radiative impact of a  $4xCO_2$  perturbation more potent. The reverse is true in the ‘Strat  $O_3 \times 1.5$ ’ case. In relation to spectral overlap,  $O_3$  itself possesses two fundamental absorption bands in the TIR around  $9.6 \mu m$  and  $14.27 \mu m$ , with a relatively strong band formed by overtone and combination transitions centered at  $4.75 \mu m$ . As stratospheric  $O_3$  concentrations increase (decrease), TIR  
235 absorption at these wavelengths also increases (decreases) to an extent that depends on the level of band saturation and the abundance of other gases absorbing at these wavelengths. For  $CO_2$ , the main TIR bands lie in the window regions of the  $H_2O$  spectrum, with absorption centered at  $4.3 \mu m$  and  $15 \mu m$  (the latter of which is highly significant due to its proximity to the peak of blackbody distribution for the Earth’s effective emitting temperature). Weaker bands also occur near  $10 \mu m$ . Regions of spectral overlap between  $O_3$  and  $CO_2$  therefore arise at several wavelengths; at  $15 \mu m$  the strength of  $CO_2$  absorption largely masks the radiative effect of  $O_3$  at  $14.27 \mu m$  and absorption by both gases at  $4.75 \mu m$  and  $4.3 \mu m$  has little impact given their  
240 location further away from the peak of Earth’s blackbody distribution. However, decreased (increased) stratospheric  $O_3$  concentration leads to weakened (strengthened) absorption at  $9.6 \mu m$  that can enhance (mute) absorption by  $CO_2$  at  $10 \mu m$ . Combining the effect of base-state stratospheric temperature and spectral overlap, a  $4xCO_2$  perturbation therefore results in an enhancement of the IRF in the ‘Strat  $O_3 \times 0.5$ ’ case relative to the ‘standard’ experiment. Correspondingly, an increase in stratospheric  $O_3$  has the opposite (albeit evidently weaker) effect.

245

In discussion of the potential climate implications of their findings, He et al. (2023) suggest that  $O_3$  depletion since the 1970s could have led to a strengthening of TOA  $CO_2$  IRF due to the cooling of the lower stratosphere associated with  $O_3$  loss. They theorise that the combined effect of  $O_3$  depletion and  $CO_2$  increase should produce a larger  $CO_2$  ERF and a greater surface warming than model experiments that impose these perturbations separately. They calculate the indirect surface warming effect  
250 of  $O_3$  loss by differencing surface temperature anomalies between two such sets of experiments (historical forcing between 1985-2014 vs the sum of all historical forcings between 1985-2014 imposed independently) and infer that the sign and spatial distribution of the nonlinear warming contribution of  $O_3$  loss to  $CO_2$  IRF is consistent with the base-state dependence of IRF. As shown above, we demonstrate that a highly idealised reduction in stratospheric  $O_3$  does lead to an enhancement of  $4xCO_2$  IRF. However, we find that this does not significantly affect the magnitude of ERF, largely because the magnitude of  $A_{T_{Strat}}$   
255 remains the same size. Figure S3 (see Supplement) confirms this result with additional and identical simulations performed CESM2 (see also Text S2 and Fig. S2).



## 5 Conclusions

Here we demonstrate that accurate calculations of IRF require the use of host-model radiative transfer calculations or online double-call simulations. Inferring IRF indirectly as the residual of ERF and the sum of adjustments can result in the erroneous estimation of its magnitude which introduces further uncertainty into the exact nature of inter-model spread in CO<sub>2</sub> ERF. We also show that increasing and decreasing stratospheric O<sub>3</sub> by 50% results in a strong warming and cooling of stratosphere, with the peak change in temperature in each experiment reaching around 6 K and -9 K, respectively. Despite the sizeable effect on stratospheric temperature, these highly idealised changes in O<sub>3</sub> concentration do not result in a correspondingly large spread in the magnitude of stratospheric temperature adjustment or 4xCO<sub>2</sub> ERF. Instead, these experiments demonstrate a dominant impact on the magnitude of IRF, chiefly due to the impact on base-state stratospheric temperature and the spectral overlap of CO<sub>2</sub> and O<sub>3</sub>, whereby for example, decreasing stratospheric O<sub>3</sub> weakens absorption by O<sub>3</sub> at 9.6 μm and enhances CO<sub>2</sub> absorption at 10 μm, resulting in a strengthening of the greenhouse effect of CO<sub>2</sub> following a quadrupling of its concentration. Given that such large changes in stratospheric O<sub>3</sub> do not yield a significant impact on 4xCO<sub>2</sub> ERF, our results suggests that inter-model differences in stratospheric O<sub>3</sub> concentration are not predominantly responsible for inter-model spread in CO<sub>2</sub> forcing.

*Code availability.* NorESM2 can be downloaded from <https://doi.org/10.5281/zenodo.3905091> (Seland et al., 2020). CESM2 can be downloaded from <https://www.cesm.ucar.edu/models/cesm2> (Danabasoglu et al., 2020).

*Data availability:* The CESM-CAM5 radiative kernels are freely available at <https://doi.org/10.5065/D6F47MT6> (Pendergrass et al., 2018). The ECMWF-Oslo kernels are freely available at <https://github.com/ciceroOslo/Radiative-kernels.git> (Myhre et al., 2018). The HadGEM3-GA7.1 kernels are freely available at <https://doi.org/10.5281/zenodo.3594673> (Smith et al., 2020b).

*Author contributions.* GM and REB designed the study. REB performed the simulations, with supporting simulations performed by GM. REB and GM analysed the data. REB produced the figures and was the primary writer of the manuscript with contributions from GM, DO and MS.

*Competing interests.* At least one of the (co-)authors is a member of the editorial board of Atmospheric Chemistry and Physics.

*Acknowledgements.* We thank Christopher J. Smith for his input on technical aspects of this manuscript and for his review and comments. We also thank Marit Sandstad for her technical advice on model simulations. REB and GM were supported by the European Union's Horizon 2020 research and innovation programme under grant agreement No 820829 (CONSTRAIN).



## References

- 290 Andrews, T., Gregory, J. M., and Webb, M. J.: The Dependence of Radiative Forcing and Feedback on Evolving Patterns of Surface Temperature Change in Climate Models, *Journal of Climate*, 28, 1630-1648, <https://doi.org/10.1175/JCLI-D-14-00545.1>, 2015.
- Andrews, T., Smith, C. J., Myhre, G., Forster, P. M., Chadwick, R., and Ackerley, D.: Effective Radiative Forcing in a GCM With Fixed Surface Temperatures, *Journal of Geophysical Research: Atmospheres*, 126, e2020JD033880, <https://doi.org/10.1029/2020JD033880>, 2021.
- 295 Boucher, O., D. Randall, P. Artaxo, C. Bretherton, G. Feingold, P. Forster, V.-M. Kerminen, Y. Kondo, H. Liao, U. Lohmann, P. Rasch, S.K. Satheesh, S. Sherwood, B. Stevens, and X.Y. Zhang: Clouds and aerosols. In *Climate Change 2013: The Physical Science Basis. Contribution of Working Group I to the Fifth Assessment Report of the Intergovernmental Panel on Climate Change.*, 571-657, 10.1017/CBO9781107415324.016, 2013.
- 300 Chung, E.-S. and Soden, B. J.: An Assessment of Direct Radiative Forcing, Radiative Adjustments, and Radiative Feedbacks in Coupled Ocean–Atmosphere Models, *Journal of Climate*, 28, 4152-4170, <https://doi.org/10.1175/JCLI-D-14-00436.1>, 2015a.
- Chung, E.-S. and Soden, B. J.: An assessment of methods for computing radiative forcing in climate models, *Environmental Research Letters*, 10, 074004, 10.1088/1748-9326/10/7/074004, 2015b.
- 305 Collins, W. D., Ramaswamy, V., Schwarzkopf, M. D., Sun, Y., Portmann, R. W., Fu, Q., Casanova, S. E. B., Dufresne, J.-L., Fillmore, D. W., Forster, P. M. D., Galin, V. Y., Gohar, L. K., Ingram, W. J., Kratz, D. P., Lefebvre, M.-P., Li, J., Marquet, P., Oinas, V., Tsushima, Y., Uchiyama, T., and Zhong, W. Y.: Radiative forcing by well-mixed greenhouse gases: Estimates from climate models in the Intergovernmental Panel on Climate Change (IPCC) Fourth Assessment Report (AR4), *Journal of Geophysical Research: Atmospheres*, 111, <https://doi.org/10.1029/2005JD006713>, 2006.
- 310 Conley, A. J., Lamarque, J. F., Vitt, F., Collins, W. D., and Kiehl, J.: PORT, a CESM tool for the diagnosis of radiative forcing, *Geosci. Model Dev.*, 6, 469-476, 10.5194/gmd-6-469-2013, 2013.
- Danabasoglu, G., Lamarque, J.-F., Bacmeister, J., Bailey, D. A., DuVivier, A. K., Edwards, J., Emmons, L. K., Fasullo, J., Garcia, R., Gettelman, A., Hannay, C., Holland, M. M., Large, W. G., Lauritzen, P. H., Lawrence, D. M., Lenaerts, J. T. M., Lindsay, K., Lipscomb, W. H., Mills, M. J., Neale, R., Oleson, K. W., Otto-Bliesner, B., Phillips, A. S.,
- 315 Sacks, W., Tilmes, S., van Kampenhout, L., Vertenstein, M., Bertini, A., Dennis, J., Deser, C., Fischer, C., Fox-Kemper, B., Kay, J. E., Kinnison, D., Kushner, P. J., Larson, V. E., Long, M. C., Mickelson, S., Moore, J. K., Nienhouse, E., Polvani, L., Rasch, P. J., and Strand, W. G.: The Community Earth System Model Version 2 (CESM2), *Journal of Advances in Modeling Earth Systems*, 12, e2019MS001916, <https://doi.org/10.1029/2019MS001916>, 2020.
- 320 Etminan, M., Myhre, G., Highwood, E. J., and Shine, K. P.: Radiative forcing of carbon dioxide, methane, and nitrous oxide: A significant revision of the methane radiative forcing, *Geophysical Research Letters*, 43, 12,614-612,623, <https://doi.org/10.1002/2016GL071930>, 2016.
- Eyring, V., Bony, S., Meehl, G. A., Senior, C. A., Stevens, B., Stouffer, R. J., and Taylor, K. E.: Overview of the Coupled Model Intercomparison Project Phase 6 (CMIP6) experimental design and organization, *Geosci. Model Dev.*, 9, 1937-1958, 10.5194/gmd-9-1937-2016, 2016.
- 325 Forster, P., T. Storelvmo, K. Armour, W. Collins, J.-L. Dufresne, D. Frame, D.J. Lunt, T. Mauritsen, M.D. Palmer, M. Watanabe, M. Wild, and H. Zhang: The Earth's Energy Budget, Climate Feedbacks and Climate Sensitivity, in: *In Climate Change 2021: The Physical Science Basis. Contribution of Working Group I to the Sixth Assessment Report of the Intergovernmental Panel on Climate Change*, edited by: Masson-Delmotte, V., P. Zhai, A. Pirani, S.L. Connors, C. Péan, S. Berger, N. Caud, Y. Chen, L. Goldfarb, M.I. Gomis, M. Huang, K. Leitzell, E. Lonnoy, J.B.R. Matthews, T.K. Maycock, T. Waterfield, O. Yelekçi, R. Yu, and B. Zhou, Cambridge University Press, Cambridge, United Kingdom and New York, NY, USA, 923-1054, 10.1017/9781009157896.009., 2021.
- 330 Forster, P. M., Richardson, T., Maycock, A. C., Smith, C. J., Samset, B. H., Myhre, G., Andrews, T., Pincus, R., and Schulz, M.: Recommendations for diagnosing effective radiative forcing from climate models for CMIP6, *Journal of Geophysical Research: Atmospheres*, 121, 12,460-412,475, <https://doi.org/10.1002/2016JD025320>, 2016.
- 335 Gettelman, A., Mills, M. J., Kinnison, D. E., Garcia, R. R., Smith, A. K., Marsh, D. R., Tilmes, S., Vitt, F., Bardeen, C. G., McInerney, J., Liu, H.-L., Solomon, S. C., Polvani, L. M., Emmons, L. K., Lamarque, J.-F., Richter, J. H., Glanville,



- 340 A. S., Bacmeister, J. T., Phillips, A. S., Neale, R. B., Simpson, I. R., DuVivier, A. K., Hodzic, A., and Randel, W. J.:  
The Whole Atmosphere Community Climate Model Version 6 (WACCM6), *Journal of Geophysical Research:  
Atmospheres*, 124, 12380-12403, <https://doi.org/10.1029/2019JD030943>, 2019.
- Gregory, J. M., Ingram, W. J., Palmer, M. A., Jones, G. S., Stott, P. A., Thorpe, R. B., Lowe, J. A., Johns, T. C., and Williams,  
K. D.: A new method for diagnosing radiative forcing and climate sensitivity, *Geophysical Research Letters*, 31,  
<https://doi.org/10.1029/2003GL018747>, 2004.
- 345 Hansen, J., Fung, I., Lacis, A., Rind, D., Lebedeff, S., Ruedy, R., Russell, G., and Stone, P.: Global climate changes as forecast  
by Goddard Institute for Space Studies three-dimensional model, *Journal of Geophysical Research: Atmospheres*, 93,  
9341-9364, <https://doi.org/10.1029/JD093iD08p09341>, 1988.
- Hansen, J., Sato, M., Ruedy, R., Nazarenko, L., Lacis, A., Schmidt, G. A., Russell, G., Aleinov, I., Bauer, M., Bauer, S., Bell,  
N., Cairns, B., Canuto, V., Chandler, M., Cheng, Y., Del Genio, A., Faluvegi, G., Fleming, E., Friend, A., Hall, T.,  
Jackman, C., Kelley, M., Kiang, N., Koch, D., Lean, J., Lerner, J., Lo, K., Menon, S., Miller, R., Minnis, P., Novakov,  
350 T., Oinas, V., Perlwitz, J., Perlwitz, J., Rind, D., Romanou, A., Shindell, D., Stone, P., Sun, S., Tausnev, N., Thresher,  
D., Wielicki, B., Wong, T., Yao, M., and Zhang, S.: Efficacy of climate forcings, *Journal of Geophysical Research:  
Atmospheres*, 110, <https://doi.org/10.1029/2005JD005776>, 2005.
- He, H., Kramer, R. J., Soden, B. J., and Jeevanjee, N.: State dependence of CO<sub>2</sub> forcing and its implications for climate  
sensitivity, *Science*, 382, 1051-1056, doi:10.1126/science.abq6872, 2023.
- 355 Iacono, M. J., Delamere, J. S., Mlawer, E. J., Shephard, M. W., Clough, S. A., and Collins, W. D.: Radiative forcing by long-  
lived greenhouse gases: Calculations with the AER radiative transfer models, *Journal of Geophysical Research:  
Atmospheres*, 113, <https://doi.org/10.1029/2008JD009944>, 2008.
- Jeevanjee, N., Seeley, J. T., Paynter, D., and Fueglistaler, S.: An Analytical Model for Spatially Varying Clear-Sky CO<sub>2</sub>  
Forcing, *Journal of Climate*, 34, 9463-9480, <https://doi.org/10.1175/JCLI-D-19-0756.1>, 2021.
- 360 Kamae, Y. and Watanabe, M.: On the robustness of tropospheric adjustment in CMIP5 models, *Geophysical Research Letters*,  
39, <https://doi.org/10.1029/2012GL054275>, 2012.
- Marvel, K., Schmidt, G. A., Miller, R. L., and Nazarenko, L. S.: Implications for climate sensitivity from the response to  
individual forcings, *Nature Climate Change*, 6, 386-389, 10.1038/nclimate2888, 2016.
- 365 Meinshausen, M., Nicholls, Z. R. J., Lewis, J., Gidden, M. J., Vogel, E., Freund, M., Beyerle, U., Gessner, C., Nauels, A.,  
Bauer, N., Canadell, J. G., Daniel, J. S., John, A., Krummel, P. B., Luderer, G., Meinshausen, N., Montzka, S. A.,  
Rayner, P. J., Reimann, S., Smith, S. J., van den Berg, M., Velders, G. J. M., Vollmer, M. K., and Wang, R. H. J.:  
The shared socio-economic pathway (SSP) greenhouse gas concentrations and their extensions to 2500, *Geosci.  
Model Dev.*, 13, 3571-3605, 10.5194/gmd-13-3571-2020, 2020.
- 370 Myhre, G., Highwood, E. J., Shine, K. P., and Stordal, F.: New estimates of radiative forcing due to well mixed greenhouse  
gases, *Geophysical Research Letters*, 25, 2715-2718, <https://doi.org/10.1029/98GL01908>, 1998.
- Myhre, G., Kramer, R. J., Smith, C. J., Hodnebrog, Ø., Forster, P., Soden, B. J., Samset, B. H., Stjern, C. W., Andrews, T.,  
Boucher, O., Faluvegi, G., Fläschner, D., Kasoar, M., Kirkevåg, A., Lamarque, J.-F., Olivé, D., Richardson, T.,  
Shindell, D., Stier, P., Takemura, T., Voulgarakis, A., and Watson-Parris, D.: Quantifying the Importance of Rapid  
Adjustments for Global Precipitation Changes, *Geophysical Research Letters*, 45, 11,399-311,405,  
375 <https://doi.org/10.1029/2018GL079474>, 2018.
- Myhre, G., Shindell, D., Bréon, F. M., Collins, W., Fuglestad, J., Huang, J., et al. : Anthropogenic and natural radiative  
forcing, in: *Climate change 2013: The physical science basis. Contribution of Working Group I to the Fifth  
Assessment Report of the Intergovernmental Panel on Climate Change*, edited by: T. F. Stocker, D. Q., G. K. Plattner,  
M. Tignor, S. K. Allen, J. Boschung, et al. , Cambridge University Press, Cambridge, UK and New York 659–740,  
380 2013.
- Pendergrass, A. G., Conley, A., and Vitt, F. M.: Surface and top-of-atmosphere radiative feedback kernels for CESM-CAM5,  
*Earth Syst. Sci. Data*, 10, 317-324, 10.5194/essd-10-317-2018, 2018.
- Pincus, R., Buehler, S. A., Brath, M., Crevoisier, C., Jamil, O., Franklin Evans, K., Manners, J., Menzel, R. L., Mlawer, E. J.,  
Paynter, D., Pernak, R. L., and Tellier, Y.: Benchmark Calculations of Radiative Forcing by Greenhouse Gases,  
385 *Journal of Geophysical Research: Atmospheres*, 125, e2020JD033483, <https://doi.org/10.1029/2020JD033483>, 2020.
- Pincus, R., Forster, P. M., and Stevens, B.: The Radiative Forcing Model Intercomparison Project (RFMIP): experimental  
protocol for CMIP6, *Geosci. Model Dev.*, 9, 3447-3460, 10.5194/gmd-9-3447-2016, 2016.



- Pincus, R., Mlawer, E. J., Oreopoulos, L., Ackerman, A. S., Baek, S., Brath, M., Buehler, S. A., Cady-Pereira, K. E., Cole, J. N. S., Dufresne, J.-L., Kelley, M., Li, J., Manners, J., Paynter, D. J., Roehrig, R., Sekiguchi, M., and Schwarzkopf, D. M.: Radiative flux and forcing parameterization error in aerosol-free clear skies, *Geophysical Research Letters*, 42, 5485-5492, <https://doi.org/10.1002/2015GL064291>, 2015.
- Ramaswamy, V., Collins, W., Haywood, J., Lean, J., Mahowald, N., Myhre, G., Naik, V., Shine, K. P., Soden, B., Stenchikov, G., and Storelvmo, T.: Radiative Forcing of Climate: The Historical Evolution of the Radiative Forcing Concept, the Forcing Agents and their Quantification, and Applications, *Meteorological Monographs*, 59, 10.1175/AMSMONOGRAPHS-D-19-0001.1, 2019.
- Richardson, T. B., Forster, P. M., Smith, C. J., Maycock, A. C., Wood, T., Andrews, T., Boucher, O., Faluvegi, G., Fläschner, D., Hodnebrog, Ø., Kasoar, M., Kirkevåg, A., Lamarque, J.-F., Mülmenstädt, J., Myhre, G., Olivié, D., Portmann, R. W., Samset, B. H., Shawki, D., Shindell, D., Stier, P., Takemura, T., Voulgarakis, A., and Watson-Parris, D.: Efficacy of Climate Forcings in PDRMIP Models, *Journal of Geophysical Research: Atmospheres*, 124, 12824-12844, <https://doi.org/10.1029/2019JD030581>, 2019.
- Seland, Ø., Bentsen, M., Olivié, D., Toniazzo, T., Gjermundsen, A., Graff, L. S., Debernard, J. B., Gupta, A. K., He, Y. C., Kirkevåg, A., Schwinger, J., Tjiputra, J., Aas, K. S., Bethke, I., Fan, Y., Griesfeller, J., Grini, A., Guo, C., Ilicak, M., Karset, I. H. H., Landgren, O., Liakka, J., Moseid, K. O., Nummelin, A., Spensberger, C., Tang, H., Zhang, Z., Heinze, C., Iversen, T., and Schulz, M.: Overview of the Norwegian Earth System Model (NorESM2) and key climate response of CMIP6 DECK, historical, and scenario simulations, *Geosci. Model Dev.*, 13, 6165-6200, 10.5194/gmd-13-6165-2020, 2020.
- Sherwood, S. C., Bony, S., Boucher, O., Bretherton, C., Forster, P. M., Gregory, J. M., and Stevens, B.: Adjustments in the Forcing-Feedback Framework for Understanding Climate Change, *Bulletin of the American Meteorological Society*, 96, 217-228, <https://doi.org/10.1175/BAMS-D-13-00167.1>, 2015.
- Smith, C. J., Kramer, R. J., Myhre, G., Alterskjær, K., Collins, W., Sima, A., Boucher, O., Dufresne, J. L., Nabat, P., Michou, M., Yukimoto, S., Cole, J., Paynter, D., Shiogama, H., O'Connor, F. M., Robertson, E., Wiltshire, A., Andrews, T., Hannay, C., Miller, R., Nazarenko, L., Kirkevåg, A., Olivié, D., Fiedler, S., Lewinschal, A., Mackallah, C., Dix, M., Pincus, R., and Forster, P. M.: Effective radiative forcing and adjustments in CMIP6 models, *Atmos. Chem. Phys.*, 20, 9591-9618, 10.5194/acp-20-9591-2020, 2020a.
- Smith, C. J., Kramer, R. J., Myhre, G., Forster, P. M., Soden, B. J., Andrews, T., Boucher, O., Faluvegi, G., Fläschner, D., Hodnebrog, Ø., Kasoar, M., Kharin, V., Kirkevåg, A., Lamarque, J.-F., Mülmenstädt, J., Olivié, D., Richardson, T., Samset, B. H., Shindell, D., Stier, P., Takemura, T., Voulgarakis, A., and Watson-Parris, D.: Understanding Rapid Adjustments to Diverse Forcing Agents, *Geophysical Research Letters*, 45, 12,023-012,031, <https://doi.org/10.1029/2018GL079826>, 2018.
- Smith, C. J., Kramer, R. J., and Sima, A.: The HadGEM3-GA7.1 radiative kernel: the importance of a well-resolved stratosphere, *Earth Syst. Sci. Data*, 12, 2157-2168, 10.5194/essd-12-2157-2020, 2020b.
- Soden, B. J., Collins, W. D., and Feldman, D. R.: Reducing uncertainties in climate models, *Science*, 361, 326-327, doi:10.1126/science.aau1864, 2018.
- Soden, B. J., Held, I. M., Colman, R., Shell, K. M., Kiehl, J. T., and Shields, C. A.: Quantifying Climate Feedbacks Using Radiative Kernels, *Journal of Climate*, 21, 3504-3520, <https://doi.org/10.1175/2007JCLI2110.1>, 2008.
- Zelinka, M. D., Andrews, T., Forster, P. M., and Taylor, K. E.: Quantifying components of aerosol-cloud-radiation interactions in climate models, *Journal of Geophysical Research: Atmospheres*, 119, 7599-7615, <https://doi.org/10.1002/2014JD021710>, 2014.
- Zhang, M. and Huang, Y.: Radiative Forcing of Quadrupling CO<sub>2</sub>, *Journal of Climate*, 27, 2496-2508, <https://doi.org/10.1175/JCLI-D-13-00535.1>, 2014.